# The conserved core component EsaA mediates bacterial killing by the type VIIb secretion system

**Nicole Mietrach**
University of Würzburg
**Diana Damián-Aparicio**
Spanish National Center for Biotechnology
**Michail Isupov**
University of Exeter
**Marcin Krupka**
Spanish National Center for Biotechnology
**Daniel Lopez** ( dlopez@cnb.csic.es )
Spanish National Research Council https://orcid.org/0000-0002-8627-3813
**Sebastian Geibel** ( sebastian.geibel@uni-wuerzburg.de )
University of Würzburg https://orcid.org/0000-0003-0068-680X

**Article**

**Keywords:** type VII secretion system, ESAT-6 like secretion system, EsaA, Staphylococcus aureus USA300, MRSA, Staphylococcus aureus NCTC8325, bacterial competition, biofilm, membrane lysis

**Posted Date:** November 3rd, 2020

**DOI:** https://doi.org/10.21203/rs.3.rs-95626/v2

# Abstract

Type VII secretion systems (T7SS) are employed by Gram-positive bacteria to infect the host or to intoxicate bacterial competitors. Bacterial killing mediated by other secretion systems involves the assembly of large, extracellular structures promoting toxin delivery into bacterial competitors. However, such extracellular structures are not known for T7SS nor is it known whether the secreted toxins have cell-penetrating properties. Here, we used a multi-drug resistant *Staphylococcus aureus*, one of the most relevant hospital-associated bacterial pathogens, to study the mechanism of bacterial killing by the T7SSb. We report the proteolysis-resistant, extracellular structure of the EsaA core component, which is an integral part of the membrane-embedded T7SSb secretion machine. The extracellular structure of EsaA has an elongated antenna-like shape providing an explanation how the T7SSb spans the staphylococcal cell wall. We demonstrate that the extracellular structure of EsaA has an essential function in secretion and contributes to the killing of prey bacteria. We show that the bactericidal activity of EsaA can be attributed to a membrane-damaging activity that leads to the permeabilization of phospholipid bilayers and could facilitate the delivery of antibacterial toxin into bacterial competitors. The structural similarity of the EsaA tip domain to bacterial lectins and human integrins suggests an additional function of EsaA in cell adhesion during infection or in targeting of bacterial competitors.


# Significance

The success of *Staphylococcus aureus* as human pathogen lies partly in its ability to resist antibiotic treatments as well as to outcompete host skin microbiota. Here we used a community-acquired multi-drug resistant *Staphylococcus aureus (*CA-MRSA), responsible for most of the hospital-associated infections, to study to the structure and function of the EsaA core membrane component, which is an essential part of the T7SSb secretion machine. We show the T7SSb secretion apparatus assembles a cell envelope spanning structure with phospholipid membrane lysing activity capable of killing bacterial competitors. Our work provides first insights into the mechanism of bacterial killing by T7SSb and will be useful for the design of antimicrobial strategies that aim to interfere with host colonization strategies of *S. aureus.*

# Introduction

Gram-positive bacteria use type VII secretion systems (T7SS) to transport effector proteins across their complex cell wall. T7SS are classified in two distinct groups, T7SSa and T7SSb. The T7SSa is found in high G+C Gram-positive bacteria or Actinobacteria. In this class, T7SSa has been studied in mycobacteria, in which it is known to play an important role in the pathogenicity of *Mycobacterium tuberculosis.* The T7SSb is widespread in low G+C Gram-postive bacteria or Firmicutes. In this class, T7SSb also contributes to pathogenicity, as it promotes abscess formation in *Staphylococcus aureus* infections (1–4). However, a distingushing feature of the T7SSb is its recently discovered role in interbacterial competition (5–9).

*Staphylococcus aureus* is one of the most threatening hospital-associated pathogens. It innocuously colonizes the nasopharynx and skin of many individuals and it becomes pathogenic only when the skin barrier or the mucous membrane is compromised and the pathogen internalizes into the body. *S. aureus* has the capacity to colonize different organs and cause diverse types of infections. Most of the *S. aureus* strains cause severe infections when associated with bones or soft tissues, which occasionally progress to life-threatening diseases, such as necrotizing fasciitis or pneumonia, causing a large variety of infections with a ~20% mortality rate in clinical contexts (10, 11).

One critical aspect of *S. aureus* success as a pathogen is its ability to acquire resistance to antibiotics (12, 13). The widespread use of -lactam antibiotics (e.g. methicillin), caused the evolution of *S. aureus* strains in clinical settings that resist a wide variety of -lactam antibiotics, known as methicillin-resistant *S. aureus (*MRSA). MRSA infections are difficult to treat and show a high mortality rate in clinical settings. A large number of the MRSA strains are now endemic in hospitals, as they were able to outcompete classical antibiotic-sensitive strains as well as other species from human microbiota (14).

Besides its role in staphylococcal pathogenicity, recent studies uncovered a role of T7SSb in intra- and interbacterial competition in members of Firmicutes *S. aureus, S. intermedius* and *B. subtilis* (5–9). In relation to the role of T7SSb in intra- and interbacterial competition, six protein secretion systems (T1SS, T3SS, T4SS, T5SS, T6SS, T7SSb) and the cell wall associated protein family WapA are currently known to mediate contact dependent protein toxin delivery (Fig. S1A, B) (15–17). These systems can be distinguished by their toxin delivery mechanism. For instance, the toxins of the T5SS and the cell wall associated WapA toxin family are translocated by the TAT translocon. These toxins exhibit filamentous structures, which protrude from the cell surface to interact with receptors on target cells. Upon proteolytic cleavage, the toxin domain is thought to gain entry into the target cell. In contrast, T1SS, T3SS, T4SS and T6SS assemble a molecular device for toxin delivery that penetrates bacterial or eukaryotic target cells (16). The T1SS forms adhesive aggregates on the cell surface to either penetrate the cell wall of prey bacteria or serve as condiut for the delivery of toxins into the target cell. The T3SS uses a needle-like device to penetrate the cell wall of bacterial competitors and inject toxins. The T4SS assembles a pilus that is thought to mediate recognition of and attachment to target cells or probably serves as a conduit for effector proteins. The T6SS operates a contractile sheath that propells a needle tip loaded with effector proteins towards the target cell that are released upon cell wall penetration. However, the molecular structure that is used by T7SSb apparatus to interact with or penetrate target cells is unknown, nor is it known whether the secreted antibacterial toxins themselves mediate cell contact and entry.

Although the organization of the T7SSb apparatus is far from being understood, the role of several proteins in T7SSb organization has been addressed. The membrane embedded T7SSb core machinery consists of four conserved membrane proteins EsaA, EssA, EssB and EssC that are required for substrate secretion (17) (Fig. S1A). Little is known how T7SSb machines work, because structural data are currently limited to only two membrane components EssB and EssC. The motor protein EssC is the only ATPase of the membrane embedded secretion complex and the only membrane component shared with T7SSa. EssC targets substrates in the cytosol and provides the energy for their secretion (5, 18–20). More

recently, it has been shown that EssB may also play a role in substrate targeting (9). Nonetheless, the functions of EssA and EsaA are still unknown and therefore, a general map of the T7SSb organization is currently missing.

EsaA is predicted to consist of six α-transmembrane helices (TMH) and an extremely large extracellular segment, consisting of ca. 750 amino acids (21). Protease shaving experiments showed that EsaA is the only surface exposed component of the T7SSb secretion apparatus in *S. aureus* (22). Therefore we hypothesized that EsaA must play an exclusive role in the organization and function of the TS77b in Staphylococci. In contrast, structural information confirmed that the EssB extracellular domain is too small to span the cell wall whereas the only other membrane component with a predicted extracellular domain, EssA (<15 kDa), is too small in terms of molecular weight to cross the cell wall (9, 23).

A growing number of antibacterial toxins of the polymorphic (F/L)XG family has been identified as novel substrates of the T7SSb (5–9). These antibacterial toxins are bound to intracellular antitoxins, which neutralize their toxic activity and in addition provide protection in intra-species competition (5, 7–9). Two toxins have been characterized in *S. aureus* so far: the antibacterial nuclease toxin EsaD (5, 24) and the membrane-depolarizing toxin TspA, which shows activity against prokaryotic and eukaryotic cells (6). EsaD is the best-characterized toxin so far. EsaD is bound to antitoxin EsaG in the cytoplasm and targeted to the motor ATPase by chaperone EssE for transport (5, 18). EssE is also required for the secretion of a set of four small Esx substrates (EsxA, EsxB, EsxC, EsxD) belonging the WxG100 protein family in an yet unknown manner (18).

In the close-relative bacterium *Bacillus subtilis,* the T7SSb plays a role in conjugation independent of T7SSb activity (25) and it is currently attributed to the core membrane component YueB (an EsaA homolog). YueB serves as receptor for bacteriophage SPP1 indicating surface exposure (25) and has a large predicted extracellular domain, similar to EsaA and therefore could mediate cell-to-cell contact during bacterial conjugation.

The possible implication of YueB in mediating cell-to-cell contact along with the finding that EsaA and YueB are surface exposed, led to our working hypothesis that EsaA is involved in the contact dependent killing of bacterial competitors while at the same time building a trans-envelope structure for substrate secretion. As no structural and functional information was available, we set out to determine the extracellular structure of EsaA and investigate its biological function in promoting cell-to-cell contact against competing bacteria.

# Results

Full-length EsaA forms dimers in the membrane of *S. aureus (*26). Consistent with this, we recently identified and purified a large proteolytic resistant fragment (amino acids 275–689) of the extracellular segment of EsaA (EsaAex hereafter) that forms dimers in solution (21). We initiated the structure determination of EsaAex to gain insights into its function (Fig. S1C). A selenomethionine derivative of EsaAex enabled the phase determination and the generation of a model at 3.8 Å resolution (Table 1). The

presence of non-crystallographic symmetry and the high solvent content enabled the generation of an electron density map featuring side chain information and enabled *de novo* modeling of the rigid core of EsaAex (amino acids 308–649) with confident threading of residues 334–624 in all eight monomers (Fig. S2).

The crystal structure of EsaAex shows a tight dimer in parallel orientation, with a slightly bent, antenna-like shape and a length of ~ 170 Å (Fig. 1A, B). The EsaAex dimer comprises a linear array of a ß-sheet domain (B) followed by two different helical domains (H1 + H2). The localization of N- and C-termini at the H1 domain shows that H1 is closest to the membrane while the ß-sheet domain is most distant from it. The proximity of N- and C-termini suggests that the proteolytic sensitive residues that are not present in the EsaAex structure and that connect EsaAex to the EsaA membrane domain, would further extend the overall length of the extracellular EsaA structure.

Several independent studies have reported diameters of the *S. aureus* cell wall in the range from 180–420 Å (27–29). The elongated shape of EsaAex provides an explanation how full-length EsaA spans the cell wall of *S. aureus* and becomes surface exposed (22).

The ß-sheet domain of EsaAex forms two opposing antiparallel ß-sheets made of seven ß-strands. α-helix 7 is inserted between ß-strands five and six and an extended loop, termed loop 7, is present between ß-strands 6 and 7. In the EsaAex dimer, ß-strand 7 comprises the dimerization interface by formation of a parallel ß-sheet (Fig. 2A).

The helical domains H1 and H2 consist of 4 α-helices each. In H2 α-helix 3 forms the dimerization interface with the neighboring H2 domain while in H1 all four helices form the dimerization interface. In monomer 2, α-helix 3 of domain H1 is broken into two smaller helices (α3, α3'; Fig. S3) that are connected through a flexible loop causing the observed bent overall structure of the EsaAex dimer.

We used the DALI server to compare EsaAex with structures in the protein database (pdb) (30). Our search revealed structural similarity of the ß-sheet domain to bacterial lectins and human integrins (Table 2; Fig. 2B). Both, lectins and integrin, have important functions in extracellular matrix recognition and cell adhesion. Lectins are found in adhesive surface structures such as pili. They recognize and bind to specific carbohydrates of the target cells (prokaryotic or eukaryotic). Integrins are cell adhesion receptors of eukaryotes. They bind to the extracellular matrix (ECM) and they attach the cell cytoskeleton to the ECM.

The structural comparison showed that potential receptors binding sites vary across the conserved protein fold or require additional structural elements for receptor binding (Fig. 2B; Fig. S3). The Fhb lectin from *Streptococcus suis* is most closely related to EsaAex (Z-score 6.9; Root Mean Square Deviation [RMSD] 3.1Å over 92 aligned Cα positions) and superimposes with all seven ß-strands of the monomeric EsaAex ß-sheet domain. Unlike EsaAex, Fhb exhibits two short α-helices that form together with a concave ß-sheet the binding pocket for the α-D-galactopyranose-(1–4)-ß-D-galactopyranose receptor. In each EsaAex monomer the concave ß-sheet has an electronegative surface potential. Each monomer

could therefore bind two α-helices with electropositive surface potential in the same orientation as observed for Fhb (Fig. 2C). The electronegative loop 7 could provide the flexibility required to fit protein ligands (Fig. 2C).

The structural similarity to bacterial lectins and eukaryotic integrins further supports a role of EsaA in mediating cell-to-cell contact. To investigate the biological function of EsaA, we replaced EsaAex with an in frame insertion of three successive flag tags in the CA-MRSA clinical isolate USA300 and investigated the secretion of substrate EsxC into the culture medium as a proxy for toxin secretion (Fig. 3A-C).

The *esaAex* deletion had a limited effect on the production of downstream-encoded substrate *esxC* and the downstream-encoded membrane component *essB* in comparison to the wild type *S. aureus* USA300 (Fig. 3B). Nonetheless, the absence of EsaAex caused a defect in the secretion of EsxC, as it was not possible to detect it in the culture supernatants (Fig. 3D). This result indicates that the extracellular domain of EsaA has an essential function that is directly or indirectly related to secretion. This could be the stabilization or the assembly of a cell wall spanning structure enabling the directed transport of substrates through the peptidoglycan layer.

Previous studies in the close-relative bacterium *B. subtilis* implicated that the EsaA homolog YueB in mediating cell-to-cell contact required for bacterial conjugation. Based on this, we hypothesized that EsaA of *S. aureus* is involved in contact dependent killing of bacterial competitors. To test this hypothesis, we set up bacterial competition assay (Fig. 4A, B), in which *S. aureus* USA300 Δ*esaAex* was co-cultured with the *S. aureus* clinical isolate NCTC8325 in relation 1:1 and after overnight incubation, prey survival rates were calculated after serial dilution plating. We used a derivate of the NCTC8325 strain as prey bacterium in this competition assay, a corneal ulcer isolate from a sepsis patient that shows antibiotic sensitivity (MSSA) (31). MRSA strains have displaced MSSA strains in clinic and now MRSA strains are endemic in hospitals. The competition assay showed that wild type *S. aureus* USA300kills *S. aureus* NCTC8325 very efficiently as no colonies of *S. aureus* NCTC8325 were detected after overnight co-culture incubation. In contrast, we observed significantly higher survival rates of the NCTC8325 strain when it was co-cultured with *S. aureus* USA300 Δ*esaAex* (13).

To investigate whether the higher survival rates can be attributed to the secretion defect of *S. aureus* USA300 Δ*esaAex* or to the absence of the extracellular EsaAex, we compared *S. aureus* USA300 Δ*esaAex* with *S. aureus* USA300 Δ*essC* using our competition assay. *S. aureus* USA300 Δ*essC* carries a seamless genetic deletion of the motor ATPase EssC and is also unable to secrete effector proteins, but it expresses a full-length EsaA (19, 32). In this case, the competition assay showed a very efficient capacity of *S. aureus* USA300 Δ*essC* to kill the prey bacterium, comparable to that of the wild type *S. aureus* USA300, suggesting that the inability of USA300 Δ*esaAex* to kill the prey bacterium is likely due to the absence of the extracellular EsaAex. To support this finding further, we assessed the effect of secretion activity on bacterial killing. We complemented *S. aureus* USA300 Δ*essC* with plasmids encoding recently studied EssC variants carrying point mutations in either the substrate binding pocket (L1356A, S1374A, L1356A/S1374A) or the Walker B motif (D1379N or D1380A) in the nucleotide-binding pocket of the

EssC-D3 ATPase domain (Fig. 4C, D). We recently showed that complementation of *S. aureus* USA300 Δ*essC* with EssC D1379A boosts secretion, while EssC D1380A, L1356A, S1374A and L1356A/S1374A cannot restore secretion (19). All complemented strains showed a similar behavior as the *S. aureus* USA300 Δ*essC* in the competition assay. We noted, that the hyperactive EssC variant was more efficient in killing prey bacteria.

Overall, our results are consistent with the notion that the attenuation of *S. aureus* USA300 Δ*esaAex* can be attributed to the absence of EsaAex (Fig. 4E). Furthermore, our experiments show that T7SSb secretion plays only a minor or no role in the competitive advantage of MSSA against CA-MRSA. This was not unexpected as the gene locus of T7SSb and the peripherally encoded genes of toxin-antitoxin TspA-TsI are highly conserved between *S. aureus* USA300 and NCTC8325, although differential transcriptional regulation and protein expression between T7SSb of both strains have been reported (3). Taken together, our data show that the extracellular domain of EsaA has an essential function in protein secretion and an additional function in the killing of bacterial competitors independent of T7SSb activity.

These results further supported the idea that the observed antibacterial activity can be attributed to EsaA itself. To test this hypothesis, we added increasing concentrations of purified EsaAex to the *S. aureus* NCTC8325 static cultures and quantified bacterial growth as direct measurement of biofilm formation after 24 h incubation. We determined the ability of *S. aureus* NCTC8325 to grow adhered to submerged surfaces using the classical biofilm formation assay in 24-well titer cultures. We determined the concentration of cells adhered to the bottom of the well using crystal violet staining (33), to determine bacterial survival rate under different concentrations of purified EsaA. In this assay, bacterial survival decreased in an EsaAex concentration-dependent manner (Fig. 5A). Using static cultures, we observed EsaAex antibacterial activity in different *S. aureus* strains, including *S. aureus* USA300 (Fig. 5B). A similar antibacterial activity of EsaA was detected in *S. aureus* USA300 Δ*esaAex* static cultures when EsaAex was added to the culture medium (Fig. 5C). Altogether, these results suggest that EsaA mediates bacterial killing irrespective of the genetic background of the competitor strain, and is more likely associated with cell-to-cell contact.

We reasoned that inhibition of cell viability in static cultures is probably due to the antibacterial activity of EsaA. According to our results, the extracellular structure of EsaA shows structural similarity to bacterial lectins or human integrins. Both, lectins and integrins, recognize and avidly bind to extracellular surfaces receptors. Therefore, we postulate that the antibacterial effect of the EsaAex may be related to the alteration of the cell envelope structure that may compromise bacterial integrity.

To explore the capacity of EsaA to damage cell envelope structures, we studied the disruption of *in vitro* generated lipid membranes upon addition of purified EsaAex. Giant unilamellar vesicles (GUVs) provide an environment confined by lipid bilayers that mimics a cell, to study biological processes associated to membranes disruption that can be easily followed using confocal microscope (34, 35). Alexa488 green fluorophore was encapsulated inside the GUVs to visualize their content. After addition of EsaAex, we observed GUVs bilayers wrinkling, suggesting membrane damage. Indeed, an efflux of Alexa488 was

observed over time, which indicates that the lipid bilayer has partly lost its integrity. The addition of EsaAex buffer only did not have any noticeable effect on GUVs membrane or their content, indicating that the observed effect was caused by EsaAex membrane damage activity (Fig. 6A).

To visualize the damaging effect of EsaA on membranes in detail, we used lipid monolayers. This technique allows studying the interaction between membranes and membrane-associated proteins dispersed in solution that become confined on two-dimensional monolayer (35–37). A solution of bacterial membrane lipids was allowed to organize in a monolayer using a custom-made Teflon block system and was placed on electron microscopy grids. These grids were exposed to EsaAex solution before examining the morphology of the lipid monolayer using TEM. The addition of EsaAex buffer did not affect the monolayers. Upon addition of EsaAex we observed rapid disintegration of the monolayers in a time-dependent manner, consistent with the results obtained with GUVs (Fig. 6B).

# Discussion

The structure of the extracellular part of EsaA provides an explanation how the T7SSb spans the cell envelope. Consistent with this, we find that the extracellular segment of EsaA is crucial for secretion. The structural similarity of the EsaAex ß-sheet domain to bacterial lectins and human integrins suggests that EsaA may have an important function in targeting bacterial prey or in cell adhesion or extracellular matrix recognition of eukaryotic cells.

Here, we demonstrate that the extracellular structure of EsaA contributes to bacterial killing by damaging the plasma membrane of bacterial competitors. EsaA activity leads to the efflux of small molecules from GUVs *in vitro* making the phopsholipid bilayer permeable. It is conceivable that this membrane-damaging activity could also facilitate the access of secreted T7SSb toxins and of other antibacterial toxins into the cytosol of bacterial competitors (Fig. S5). Further research needs to elucidate the precise mechanism of plasma membrane disintegration. The EsaAex dimer bears little resemblance to the complex cell penetrating molecular devices of T3SS or T6SS indicating a different mechanism of plasma membrane penetration.

The question remains how EsaA reaches the plasma membrane of the prey bacterium. Given the length of the EsaAex crystal structure, it seems unlikely that a single EsaA molecule can span the cell wall of *S. aureus* and in addition penetrates the intact cell wall of bacterial competitors.

The secretion of cell wall degrading and remodeling hydrolases is a trademark of *S. aureus.* The most potent representative of this class of enzymes, lysostaphin, is a secreted glycylglycine endopeptidase that cleaves pentaglycine bridges in the peptidoglycan layer and causes cell lysis. Additional secreted, cell wall degrading and remodeling hydrolases have also been described. For example, protein secretion across the SEC translocon depends on the secreted N-acetylglucosaminidase SagB (38). The secretion of T7SSb substrates depends on the murein hydrolase EssH secreted by the SEC translocon. EssH is co-conserved with the T7SSb core machinery and has a function in remodeling the peptidoglycan layer to facilitate the assembly of the transenvelope structure (39). Therefore, in competitive situations it is

conceivable that the peptidoglycan layer is compromised to an extent where the plasmamembrane of *S. aureus* could become accessible. We propose that EsaA activity then permeabilizes the exposed plasmamembrane of bacterial competitors and thereby enables toxins delivery into the cytosol.

# Materials And Methods

*Generation of markerless domain deletion of EsaA in S. aureus USA300*

Cloning was performed using the Phusion Polymerase (Invitrogen) and the In-Fusion cloning Kit (Takara Bio Inc.). *S. aureus* USA300 Δ*esaAex,* missing the extracellular domain from the amino acids 275 until 869, was cloned into the pMAD vector. Two fragments, *nt 1–825 and 2067–3027,* were amplified using primer pairs X1/X2 and X3/X4 (Table S1). Overlapping regions of the primer pairs contained a $Flag_{3x}$-tag, which was included to confirm esaAΔex expression and insertion into the membrane. Both fragments were inserted into the pMAD vector, which was cleaved with restriction enzymes EcoRI and BamHI (New England Biolabs).

To generate the markerless deletion of the extracellular domain of EsaA, *esaAΔex*-pMAD was transformed into the laboratory strain *S. aureus* RN4220 and transferred by phage transduction into *S. aureus* USA300, where 1$^{st}$ and 2$^{nd}$ recombination was performed. The pMAD vector is temperature sensitive in *S. aureus* and only replicates at/less than 30 °C. The plasmid was transformed into *S. aureus* RN4220 by electroporation. 1 µg plasmid was incubated for 15 min on ice with competent *S. aureus* RN4220 cells, transferred into a pre-chilled cuvette and pulsed. Cells were recovered in 500 µl Tryptic Soy broth (TSB, Becton Dickinson) for 2 h at 30 °C. Cell suspension was spread on a TSB plate supplemented with 2 µg/ml erythromycin and 100 mM 5-Brom–4-chlor–3-indoxyl-β-D-galactopyranosid (X-Gal) and incubated for 2–3 d at 30 °C. Blue cells, containing the plasmid, were grown for 6 h at 30 °C in TSB supplemented with 2 µg/ml erythromycin. For phage production, 300 µl cells were incubated with 5 mM $CaCl_2$ for 90 sec at 57 °C and rested for 5 min at room temperature. Cells were mixed with 100 µl of ϕ11 phage lysate in dilutions $1x10^{-3}$, $1x10^{-4}$, $1x10^{-5}$ and incubated for 15–60 min at room temperature. 3 ml TSB soft agar, supplemented with 20 mM $MgSO_4$, was added to the cell suspension, mixed and spread on a LB plate, which was incubated at 30 °C overnight. Next day phage hollows were harvested by adding 3 ml TSB medium and scrapping off the soft agar layer followed by centrifugation at 4000 x g at room temperature. The supernatant was filtered twice (0.2 µm). *S. aureus* USA300 was grown for 6 h at 37 °C and prepared for phage transduction by adding $CaCl_2$ to a final concentration of 5 mM and incubation for 90 sec at 57 °C. 300 µl cell suspension were incubated with 100 µl phages containing the plasmid, for 15–60 min, spread on TSB plates supplemented with 150 µg/ml erythromycin and 100 mM X-Gal, and finally incubated for 2–3 d at 30 °C. Blue colonies of *S. aureus* USA300 carrying the pMAD plasmid were used to conduct the 1$^{st}$ and 2$^{nd}$ recombination to generate the deletion of the extracellular domain of *esaA.* This was performed as described in Yepes et al (40).

*Cloning, purification and crystallization of esaAex-pET16b*

*EsaAex*-pET16b was cloned, expressed, purified and crystallized as described in Mietrach et al (21).

EsaAex expression for SAD phasing

*EsaAex*-pET16b was transformed into BL21 Star cells for protein expression. Pre- cultures were grown for 6–8 h in LB medium supplemented with 100 µg/ml ampicillin and used to start an overnight culture at 37 °C in M9 minimal medium (1:100 dilution). The M9 minimal medium was enriched with 20 % glucose, 1 mM $MgSO_4$, 0.3 mM CaCl2 and 1 % thiamin and biotine and supplemented with 100 µg/ml ampicillin. 10 L of M9 minimal medium, including the supplements, was inoculated 1:100 with the overnight culture and grown at 30 °C by 200 rpm until $OD_{600}$ = 0.5. The culture was supplemented with 0.5 g of leucine, isoleucine, valine and selenomethionine and 1 g of lysine, threonine and phenylalanine per 10 L and incubated at 26 °C. After 15 min the culture was induced with 1 mM Isopropyl-β-D-thiogalactopyranosid (IPTG) and grown for 20 h at 26 °C by 180 rpm.

*Purification of $EsaAex_{SeMet}$*

All steps were performed at 4 °C. Cells were harvested by centrifugation using 4000 x g for 15 min. The cell pellet was resuspended in buffer A (300 mM NaCl, 50 mM Tris, pH 8.0 and 5 mM DTT) and subsequently lysed by three passages using an EmulsiFlex-C3 homogenizer. The cell lysate was centrifuged at 100 000 x g for 1 h and the supernatant supplemented with 20 mM imidazole. The supernatant was loaded onto a 5 ml HiTrap-His column (GE Healthcare) equilibrated with buffer A. The column was washed with 15 CV of buffer A, followed by 20 CV with 20 % buffer B (250 mM imidazole, 300 mM NaCl, 50 mM Tris, pH 8.0 and 5 mM DTT) and eluted with 100 % buffer B. The peak fraction was collected and Tobacco Etch Virus (TEV) protease cleavage was performed. TEV protease was mixed with protein sample in a 1:10 ratio and incubated overnight while dialyzing in buffer A supplemented with 0.5 mM EDTA. Next day, buffer A was exchanged and the sample dialyzed for 2 h. The sample was run through a HiTrap-His column and the flow-through containing cleaved $EsaAex_{SeMet}$ was collected. The TEV protease carried a His-tag and therefore TEV and non-cleaved protein were bound to the column. The flow-through was collected and concentrated using a 10 kDa concentrator (Millipore). The sample was further purified by size exclusion chromatography (SEC) via a Sephacryl S–200 HR column (GE healthcare). The column was equilibrated for 2 CV with buffer C (150 mM NaCL, 20 mM Tris, pH 8.0 and 5 mM DTT) and after sample application, eluted with 1.2 CV in buffer C.

*Crystallization of EsaAex (SeMet)*

The SEC peak fraction was concentrated to 5 or 10 mg/ml. Crystal grew in 0.2 M ammonium citrate tribasic, pH 7.0 and 20 % PEG 3350in hanging drop experiments. Crystals grew at 18 °C within 4–5 days and were cooled down at 4 °C overnight before harvesting. Crystals were equilibrated in mother liquor containing 25 % glycerol and flash frozen in liquid nitrogen.

*Structure determination of EsaAex*

Native data collection was carried out and processed as described in Mietrach et al (21). Single-wavelength anomalous dispersion data (SAD) of EsaAex (SeMet) crystals were collected at beamline P13 of the European Synchrotron Radiation Facility in Hamburg, Germany. The XDS software package (41) was used to index, integrate and scale the data to a resolution limit of 4.8 Å. Using experimental phases derived from SHELX (42), AutoBuild was used to generated a crude initial model at 3.8 Å consisting of peptide fragments (43). The resulting electron density map showed helical features. Poly alanine α-helices were placed manually and fitted into the electron density using COOT (44). After several iterative rounds of manual model building and refinement, this partial model was refined to an Rfree of 42%. This model was used for the approach described below.

Inspection of anomalous scatterer positions found by SHELX have revealed 28 strong sites which could be split into four sets of sites related by the same interatomic distances between them, with no apparent internal symmetry within these sets. These sites have allowed to find four NCS operators and define masks for multicrystal averaging with CCP4 (45) program DMMULTI (46). Multicrystal averaging between Se-SAD data set with SAD experimental phases calculated by Phaser (47) and phases from partially refined model by REFMAC5 (48) allowed to see additional features in maps.

The partial model was subjected to a phased refinement with input averaged phases (49) and rebuilt in COOT. The rebuilt models have revealed internal symmetry in the partial model, which was higher than the symmetry established from the anomalous sites. It was revealed that a described above set of Se sites corresponded to a tight EsaAex dimer. Within this dimer two domains from different monomers were related by two-fold symmetry, but symmetry operations varied between different pairs of domains due to a bend in the dimeric molecule. The maps were then subjected to eight fold multicrystal averaging with different NCS operations and masks for each domain. Improved maps have allowed *de novo* assignment of sequence for the ß-sheet domain B and helical domains H1 and H2, using known Se positions as reference points for methionine residues.

The final model was built by alternating rounds of model building with COOT and refinement with REFMAC. The refinement protocol included initial rigid body refinement, cartesian and individual B factor refinement. The Data collection and model refinement for native and SeMet data statistics are listed in Table 1.

*Secretion Assay*

*S. aureus* US300 *wildtype, esaA_Δex* and *ΔessC* pre-cultures were grown in TSB at 30 °C and used to inoculate 30 ml TSB main cultures. Cultures were started at $OD_{600}$ = 0.05 and grown at 28 °C until $OD_{600}$ = 1. Cells were centrifuged at 2770 x g at room temperature, the supernatant was filtered (0.2 µm) and precipitated using 5 % trichlocoacetic acid and rested on ice overnight. The precipitate was centrifuged by 6000 x g and the pellet was washed with 100 % ice cold acetone. Afterwards the pellet was air dried and resuspend in 100 µl 1x Laemmli buffer, 10 mM Tris, pH 8.0 for 2 h at 65 °C and left at room temperature overnight.

The cell pellet was resuspended in 20 mM Tris, 10 mM EDTA, pH 7.5, mixed with 50 µg/ml lysostaphin, 1 mM PMSF, 250 mg glass beads and incubated for 10 min at 37 °C. Afterwards the cells were lysed using the FastPrep Shaker (2x by 6.5 m/s for 45s). Samples were centrifuged for 10 min at 4000 x g and glass beads were separated from the lysate. 800 µl supernatant were centrifuged for 30 min at 100 000 x g to separate the membrane from the cytosol. The supernatant was mixed with 1x LDS samples buffer and the pellet was resuspended in 150 mM NaCl, 50 mM Tris/Cl pH 8.0 and 3 mM DTT and incubated for 10 min at 65 °C. The supernatant was analysed by western blot for EsxC-secretion (15 % SDS-PAGE, 40 µl sample, α-EsxC-rabbit) and cell lysis (12 % SDS-PAGE, 10 µl sample, α-RNA Polymerase subunit β-mouse (RNAP, ~150 kDa). The cytosolic fraction was analysed for EsxC expression (15 % SDS-PAGE, 20 µl sample, α-EsxC-rabbit) and used as loading control (12 % SDS-PAGE, 10 µl sample, α-RNAP-mouse). The membrane fraction was analysed for EsaAex expression and insertion (3–12 % Bis-Tris gel, 10 µl sample, α-Flag-mouse) and EssB expression to ensure that proteins downstream of *esaA* are not affected by the mutation (12 % SDS-PAGE, 10 µl, α-EssB-rabbit).

*Western Blot*

All antibodies used for western Blots are listed in Table S2. The western blots were performed using the wet blot system from BioRad. Samples were transferred on to PVDF membrane. Before transfer the membrane was activated for 1 min in 100 % methanol and washed for 1 min in dd$H_2O$ and transfer buffer. The sandwich device was assembled as described by the manufacturer's protocol and protein transfer was performed by 100 V for 1 h. Afterwards the membrane was blocked in 5 % milk powder TBS-Tween (0.05 %, TBS-T) for 1 h, washed 3x for 5 min and incubated overnight at 4 °C in primary antibody. Next day, the membrane was washed 3x for 5 min again and incubated for 2 h in secondary antibody. After another 3 washing steps the membrane was developed using the enhanced chemiluminescence substrate kit 12 (Pierce) and the ImageQuant LAS4000 biomolecular imager. Images were processed using ImageJ.

*Bacterial competition assay*

The indicated strains were cultured in TSB with shaking at 37ºC for 3–4 hours. Then cultures were adjusted to $OD_{600}$ of 0.1 (~$10^7$ cfu/ml) and 1 ml of attacker strain and 1 ml of prey were separately harvested and resuspended in 1 ml of TSB. 100 µl of resuspended attacker cells were mixed with the same volume of prey cells (1:1 ratio) and incubated overnight at 37ºC with shaking. Co-cultures were then serially diluted in TSB and plated in TSB agar for CFU determination. Cell differentiation between attacker (USA300) and prey (NCTC8325) strains were done checking the production of the golden pigment staphyloxanthin (USA300 is yellow pigmented while NCTC8325 is unpigmented).

*Biofilm formation assay*

*S. aureus* USA300 wildtype and ΔesaAex overnight pre-cultures were adjusted to OD600 of 0.02 in TSB supplemented with 0.25% glucose and 0.2 M MgCl2. 200 µl of the adjusted cultures were supplemented with different concentrations of purified EsaAex (500, 250, 125, 62.5 and 31.3 µg/ml) and plated per

triplicate on 96-well microtiter plates. The microtiter plates were incubated for 24 h at 37ºC with no shaking. To process the biofilm, each well was washed five times with dH2O and dried to remove the planktonic cells. The biofilm was then fixed with heat for 30 min and stained with 100 µl of 0.1% (w/v) crystal violet for 10 min at room temperature. Then it was washed five times with dH2O and dried. Finally, the biofilm was resuspended in 100 µl 33% (v/v) acetic acid for 15 min with shaking and OD595 was measured.

*Giant Unilamellar Vesicles (GUVs) preparation*

GUVs were prepared by a droplet transfer method described previously (34, 50) with the following exceptions. The lipid mixture used for their formation contained E. coli polar lipids supplemented with 0,04% rhodamine (L-alpha-phosphatidyletanolamine-N-(lissamine rhodamine B sulfonyl) (ammonium salt) (both from Avanti Polar Lipids). Free Alexa488 (2 µg/ml) was encapsulated inside GUVs to easily distinguish them from other lipid structures or mineral oil contaminants. The purified EsaA loop was added to the already formed GUVs to the final concentration of 20 µM. Images were collected with confocal multispectral Laica TCS SP8 microscope with a 63x immersion objective.

*Lipid monolayer assay*

Two-dimensional lipid monolayers were prepared using E. coli polar lipids (Avanti Polar Lipids) as previously described (35). Briefly, 0.2 µg of lipids were floated on EsaA buffer using a custom-made Teflon block and placed for 1h in a humid chamber to evaporate the chloroform. Electron microscopy grids were then placed on the monolayers with the carbon side facing the buffer (the grids cannot be glow-discharged). It was followed by the addition of EsaA loop to the final concentration of 5 µM and incubation for 0.5, 2 and 5 minutes. The corresponding grids were then negatively stained with 1% uranyl acetate and inspected using a Jeol JEM1011 transmission electron microscope and photographed with an 11-megapixel charge-coupled Gatan Erlanghsen ES1000W camera. The software used for image processing was Gatan Digital Micrograph 1.8.0.

# Declarations

*Acknowledgement*

We would like to thank Dr. Thomas Schneider at beamline 14 at the Deutsches Elektronen Synchroton (DESY) in Hamburg (Germany) and the local contact at beamline ID30-A3 at the European Synchrotorn Radiation Facility in Grenoble (France) for assistance. We also would like to thank Prof. Dr. Tracy Palmer (Centre for Bacterial Cell Biology, Newcastle University, England) for the polyclonal antibody against EssC. This project was funded by the Elite Network of Bavaria N-BM–2013–246 to SG), BayResq-Net and by MINECO (BFU2017–87873-P) to D. Lopez. M. Krupka is recipient of a MSCA fellowship 798305.

*Author contributions*

N. M., D.DA, M. I., M. K., D. L. and S. G. designed research; N. M., D.DA., M. I., D. L. and S. G. performed research; N. M., D.DA., M. I., M. K., D. L. and S. G. analyzed data; N.M, D.DA, M. I., M. K., D. L. and S. G. wrote the paper.

The authors declare that there is no conflict of interest.

# References


1.M. I. Groschel, F. Sayes, R. Simeone, L. Majlessi, R. Brosch, ESX secretion systems: mycobacterial evolution to counter host immunity. *Nat Rev Microbiol 14,* 677–691 (2016).

2.M. L. Burts, W. A. Williams, K. DeBord, D. M. Missiakas, EsxA and EsxB are secreted by an ESAT–6-like system that is required for the pathogenesis of Staphylococcus aureus infections. *Proc Natl Acad Sci U S A 102,* 1169–1174 (2005).

3.H. Kneuper *et al.,* Heterogeneity in ess transcriptional organization and variable contribution of the Ess/Type VII protein secretion system to virulence across closely related Staphylocccus aureus strains. *Mol Microbiol 93,* 928–943 (2014).

4.Y. Wang *et al.,* Role of the ESAT–6 secretion system in virulence of the emerging community-associated Staphylococcus aureus lineage ST398. *Sci Rep 6,* 25163 (2016).

5.Z. Cao, M. G. Casabona, H. Kneuper, J. D. Chalmers, T. Palmer, The type VII secretion system of Staphylococcus aureus secretes a nuclease toxin that targets competitor bacteria. *Nat Microbiol 2,* 16183 (2016).

6.F. R. Ulhuq *et al.,* A membrane-depolarizing toxin substrate of the Staphylococcus aureus type VII secretion system mediates intraspecies competition. *Proc Natl Acad Sci U S A* 10.1073/pnas.2006110117 (2020).

7.T. A. Klein, M. Pazos, M. G. Surette, W. Vollmer, J. C. Whitney, Molecular Basis for Immunity Protein Recognition of a Type VII Secretion System Exported Antibacterial Toxin. *J Mol Biol 430,* 4344–4358 (2018).

8.J. C. Whitney *et al.,* A broadly distributed toxin family mediates contact-dependent antagonism between gram-positive bacteria. *Elife 6* (2017).

9.M. Tassinari *et al.,* Central role and structure of the membrane pseudokinase YukC in the antibacterial Bacillus subtilis Type VIIb Secretion System. *bioRxiv* 10.1101/2020.05.09.085852 (2020).

10.R. M. Klevens *et al.,* Invasive methicillin-resistant Staphylococcus aureus infections in the United States. *JAMA 298,* 1763–1771 (2007).

11.S. Y. Tong, J. S. Davis, E. Eichenberger, T. L. Holland, V. G. Fowler, Jr., Staphylococcus aureus infections: epidemiology, pathophysiology, clinical manifestations, and management. *Clin Microbiol Rev 28,* 603–661 (2015).

12.H. F. Chambers, F. R. Deleo, Waves of resistance: Staphylococcus aureus in the antibiotic era. *Nat Rev Microbiol 7,* 629–641 (2009).

13.A. S. Lee *et al.,* Methicillin-resistant Staphylococcus aureus. *Nat Rev Dis Primers 4,* 18033 (2018).

14.K. M. Daly *et al.,* Production of the Bsa lantibiotic by community-acquired Staphylococcus aureus strains. *J Bacteriol 192,* 1131–1142 (2010).

15.J. L. Willett, Z. C. Ruhe, C. W. Goulding, D. A. Low, C. S. Hayes, Contact-Dependent Growth Inhibition (CDI) and CdiB/CdiA Two-Partner Secretion Proteins. *J Mol Biol 427,* 3754–3765 (2015).

16.T. A. Klein, S. Ahmad, J. C. Whitney, Contact-Dependent Interbacterial Antagonism Mediated by Protein Secretion Machines. *Trends Microbiol 28,* 387–400 (2020).

17.S. Koskiniemi *et al.,* Rhs proteins from diverse bacteria mediate intercellular competition. *Proc Natl Acad Sci U S A 110,* 7032–7037 (2013).

18.M. Anderson *et al.,* EssE Promotes Staphylococcus aureus ESS-Dependent Protein Secretion To Modify Host Immune Responses during Infection. *J Bacteriol 199* (2017).

19.N. Mietrach, D. Damian-Aparicio, B. Mielich-Suss, D. Lopez, S. Geibel, Substrate Interaction with the EssC Coupling Protein of the Type VIIb Secretion System. *J Bacteriol 202* (2020).

20.F. Jager, H. Kneuper, T. Palmer, EssC is a specificity determinant for Staphylococcus aureus type VII secretion. *Microbiology 164,* 816–820 (2018).

21.N. Mietrach, A. Schlosser, S. Geibel, An extracellular domain of the EsaA membrane component of the type VIIb secretion system: expression, purification and crystallization. *Acta Crystallogr F Struct Biol Commun 75,* 725–730 (2019).

22.A. Dreisbach *et al.,* Profiling the surfacome of Staphylococcus aureus. *Proteomics 10,* 3082–3096 (2010).

23.M. Zoltner *et al.,* The architecture of EssB, an integral membrane component of the type VII secretion system. *Structure 21,* 595–603 (2013).

24.R. J. Ohr, M. Anderson, M. Shi, O. Schneewind, D. Missiakas, EssD, a Nuclease Effector of the Staphylococcus aureus ESS Pathway. *J Bacteriol 199* (2017).

25.C. Sao-Jose, C. Baptista, M. A. Santos, Bacillus subtilis operon encoding a membrane receptor for bacteriophage SPP1. *J Bacteriol 186,* 8337–8346 (2004).

26.F. Jager, M. Zoltner, H. Kneuper, W. N. Hunter, T. Palmer, Membrane interactions and self-association of components of the Ess/Type VII secretion system of Staphylococcus aureus. *FEBS Lett 590,* 349–357 (2016).

27.X. Zhou, L. Cegelski, Nutrient-dependent structural changes in S. aureus peptidoglycan revealed by solid-state NMR spectroscopy. *Biochemistry 51,* 8143–8153 (2012).

28.W. Yuan *et al.,* Cell wall thickening is associated with adaptive resistance to amikacin in methicillin-resistant Staphylococcus aureus clinical isolates. *J Antimicrob Chemother 68,* 1089–1096 (2013).

29.K. T. Baek *et al.,* beta-Lactam resistance in methicillin-resistant Staphylococcus aureus USA300 is increased by inactivation of the ClpXP protease. *Antimicrob Agents Chemother 58,* 4593–4603 (2014).

30.L. Holm, DALI and the persistence of protein shape. *Protein Sci 29,* 128–140 (2020).

31.R. P. Novick, Genetic systems in staphylococci. *Methods Enzymol 204,* 587–636 (1991).

32.B. Mielich-Suss *et al.,* Flotillin scaffold activity contributes to type VII secretion system assembly in Staphylococcus aureus. *PLoS Pathog 13,* e1006728 (2017).

33.G. A. O'Toole, R. Kolter, Initiation of biofilm formation in Pseudomonas fluorescens WCS365 proceeds via multiple, convergent signalling pathways: a genetic analysis. *Mol Microbiol 28,* 449–461 (1998).

34.E. J. Cabre *et al.,* Bacterial division proteins FtsZ and ZipA induce vesicle shrinkage and cell membrane invagination. *J Biol Chem 288,* 26625–26634 (2013).

35.M. Krupka *et al.,* Role of the FtsA C terminus as a switch for polymerization and membrane association. *mBio 5,* e02221 (2014).

36.M. Krupka *et al.,* Escherichia coli FtsA forms lipid-bound minirings that antagonize lateral interactions between FtsZ protofilaments. *Nat Commun 8,* 15957 (2017).

37.P. Szwedziak, Q. Wang, S. M. Freund, J. Lowe, FtsA forms actin-like protofilaments. *EMBO J 31,* 2249–2260 (2012).

38.Y. G. Chan, M. B. Frankel, D. Missiakas, O. Schneewind, SagB Glucosaminidase Is a Determinant of Staphylococcus aureus Glycan Chain Length, Antibiotic Susceptibility, and Protein Secretion. *J Bacteriol 198,* 1123–1136 (2016).

39.M. Bobrovskyy, S. E. Willing, O. Schneewind, D. Missiakas, EssH Peptidoglycan Hydrolase Enables Staphylococcus aureus Type VII Secretion across the Bacterial Cell Wall Envelope. *J Bacteriol 200* (2018).

40.A. Yepes, G. Koch, A. Waldvogel, J. C. Garcia-Betancur, D. Lopez, Reconstruction of mreB expression in Staphylococcus aureus via a collection of new integrative plasmids. *Appl Environ Microbiol 80,* 3868–3878 (2014).

41.W. Kabsch, Xds. *Acta Crystallogr D Biol Crystallogr 66,* 125–132 (2010).

42.G. M. Sheldrick, A short history of SHELX. *Acta Crystallogr A 64,* 112–122 (2008).

43.P. V. Afonine *et al.,* Towards automated crystallographic structure refinement with phenix.refine. *Acta Crystallogr D Biol Crystallogr 68,* 352–367 (2012).

44.P. Emsley, B. Lohkamp, W. G. Scott, K. Cowtan, Features and development of Coot. *Acta Crystallogr D Biol Crystallogr 66,* 486–501 (2010).

45.M. D. Winn *et al.,* Overview of the CCP4 suite and current developments. *Acta Crystallogr D Biol Crystallogr 67,* 235–242 (2011).

46.K. Cowtan, Recent developments in classical density modification. *Acta Crystallogr D Biol Crystallogr 66,* 470–478 (2010).

47.A. J. McCoy, L. C. Storoni, R. J. Read, Simple algorithm for a maximum-likelihood SAD function. *Acta Crystallogr D Biol Crystallogr 60,* 1220–1228 (2004).

48.G. N. Murshudov *et al.,* REFMAC5 for the refinement of macromolecular crystal structures. *Acta Crystallogr D Biol Crystallogr 67,* 355–367 (2011).

49.N. S. Pannu, G. N. Murshudov, E. J. Dodson, R. J. Read, Incorporation of prior phase information strengthens maximum-likelihood structure refinement. *Acta Crystallogr D Biol Crystallogr 54,* 1285–1294 (1998).

50.E. J. Cabre *et al.,* The Nucleoid Occlusion SlmA Protein Accelerates the Disassembly of the FtsZ Protein Polymers without Affecting Their GTPase Activity. *PLoS One 10,* e0126434 (2015).

51.P. V. Afonine *et al.,* FEM: feature-enhanced map. *Acta Crystallogr D Biol Crystallogr 71,* 646–666 (2015).

# Tables

**Table 1. Data collection & refinement statistics**

| Data Set | EsaA nat (pdb IDX) REF | EsaAex (SeMet-SAD) |
|---|---|---|
| Wavelength (Å) | 0.9677 | 0.9766 |
| Resolution Range (Å) | 61.33-3.78 (3.86-3.78) | 174.50-4.80 |
| Space group | $P4_12_12$ | $P4_12_12$ |
| Cell dimension a, b, c (Å); α=β=γ (°) | 196.9,196.9, 368.0, 90, 90, 90 | 197.9, 197.9, 370, 90, 90, 90 |
| Molecules/asymmetric unit | 8 | 8 |
| $R_{meas}$ (%) | 30.6 (487.5) | 25.9 (420.1) |
| I/σI | 6.2 (0.6) | 11.06 (0.97) |
| Completeness (%) | 100 (100) | 100 (99.9) |
| Multiplicity | 13.8 (14.1) | 41.92 (29.14) |
| CC1/2 | 0.998 (0.451) | 0.998 (0.657) |
| Number of measured reflections | 1,011,724 (63,021) | |
| Number of unique reflections | 73,115 (4,167) | 2883131(68770) |
| $R_{work}$ (%) | 21.8 | |
| $R_{free}$ (%) | 27.0 | |
| Average B factors ($Å^2$) | 215.4 | |
| Number of atoms (nonhydrogen) | 21,512 | |
| Rmsd bond lengths (Å) | 0.007 | |
| Rmsd bond angles (°) | 1.904 | |

The numbers in parentheses represent for the highest resolution shells.

**Table 2. Structural comparison of the ß-sheet domain to proteins in the pdb database.** Pairwise structural comparison of the ß-sheet domain monomer were carried out by the DALI protein structure comparison server (30). The table contains a select number of structures with RMSD <4 Å and Z-scores between 5-7.

| Protein | Function | Pdb code-chain | Z-score | RMSD [Å] | Aligned Cα |
|---|---|---|---|---|---|
| Fhb bound to Galα1-ß4Gal, *Streptococcus suis* | Cell adhesion | 5boa-E | 6.9 | 3.1 | 92 |
| CFA fimbrial subunit E of enterotoxigenic *E. coli* | Cell adhesion | 3vac-A | 6.1 | 3.6 | 94 |
| β-glucosidase I, *Kluyveromyces marxianus* | Hydrolase | 3abz-B | 6.0 | 2.5 | 74 |
| FMIH (F9 pilus) bound to ortho-biphenyl-2'-carboxyl N-acetyl-beta-galactosaminoside, *E. coli UTI89* | Cell adhesion | 6as8-A | 5.8 | 3.9 | 89 |
| SadP adhesion, *Streptococcus suis* | Cell adhesion | 6yro-D | 5.8 | 3.3 | 96 |
| Integrin aIIBb3 | Cell adhesion | 3fcs-C | 5.8 | 3.8 | 95 |
| F9 Pilus, lectin domain, *E. coli UTI89* | Cell adhesion | 6aow-A | 5.7 | 3.9 | 88 |
| GspB platelet binding protein | Cell adhesion | 3qc5-X | 5.7 | 3.7 | 87 |
| Lectin, *Pleurotus ostreatus* | Cell adhesion | 6t0a-A | 5.6 | 3.0 | 79 |
| β-galactosidase in complex with galactose, *Streptococcus pneumoniae* | Hydrolase | 4e8c-A | 5.6 | 2.7 | 80 |
| Leukocyte integrin aLB2 bound to 2-acetamido-2-deoxy-beta-D-glucopyranose | Cell adhesion | 5e6s-D | 5.5 | 2.8 | 75 |
| α-L-rhamnosidase, *Aspergillus terreus* | Hydrolase | 6gsz-A | 5.4 | 3.1 | 83 |
| Ephrin type-A receptor 2 in complex with BA-WLA-YSKbio peptide | Transferase | 6nkp-A | 5.3 | 2.8 | 72 |
| Cea1A in complex with Chitobiose, *Komagataella pastoris* | Adhesion protein | 5a3m | 5.2 | 3.1 | 76 |
| Integrin AlphaIIbBeta3 bound to 2-acetamido-2-deoxy-beta-D-glucopyranose | Cell adhesion | 2vdo-B | 5.1 | 2.9 | 77 |

# Figures

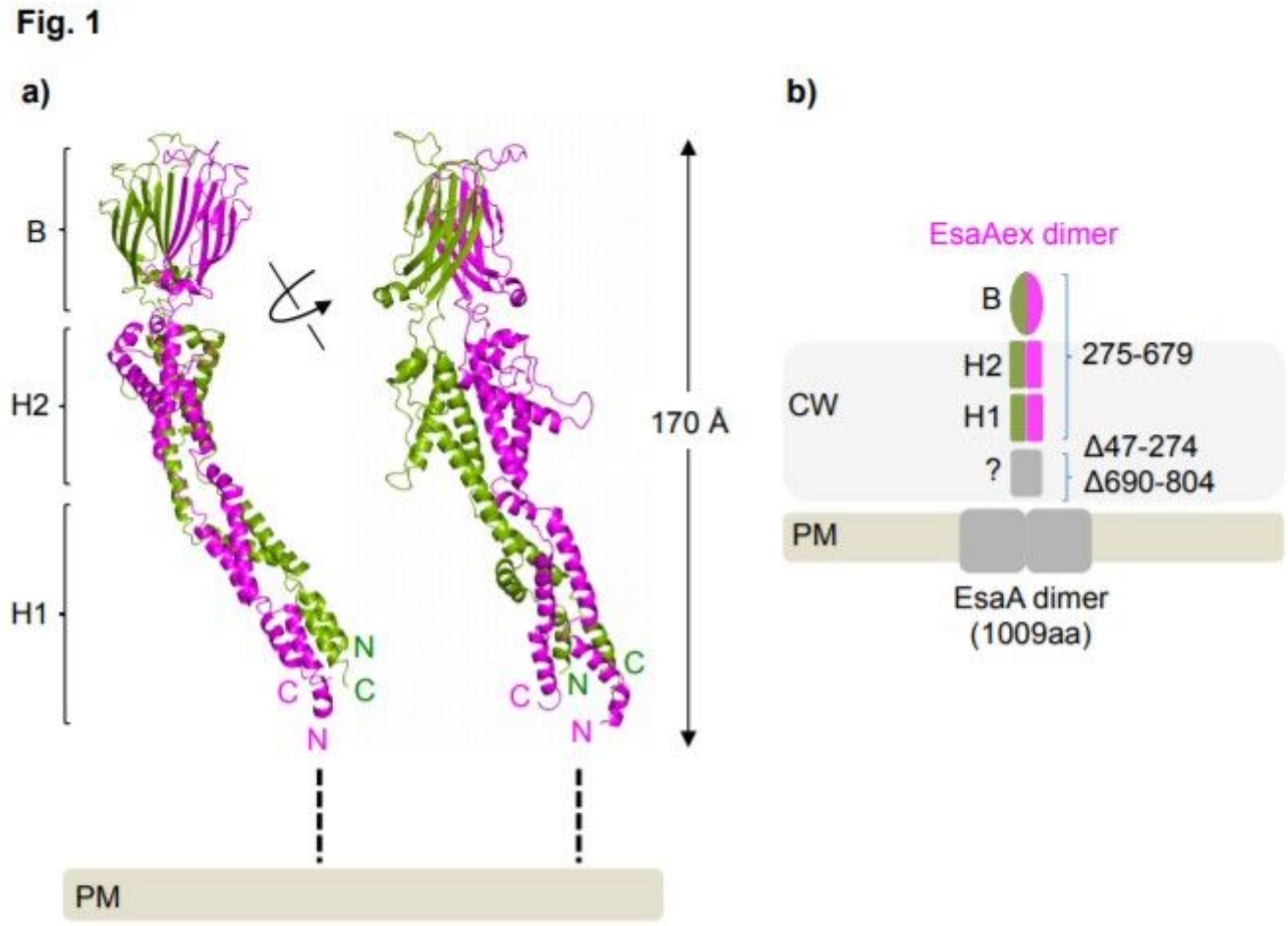


## Figure 1

The X-ray structure of the EsaAex dimer. A) The EsaAex dimer forms a tight dimer, which consists of a ß-sheet domain (B) and two consecutive helical domains (H1, H2). The EsaAex dimer has an overall length of ~ 170Å. Monomer 1 and 2 are shown in green and pink, respectively. B) Topology diagram of EsaA (1-1008 amino acids) indicating transmembrane domain (grey, amino acids 1-46; 805-1009) and the extracellular segment (green/pink/grey, amino acids 47-804). The proteolytic resistant EsaAex (green/pink) comprises amino acids 275-679.

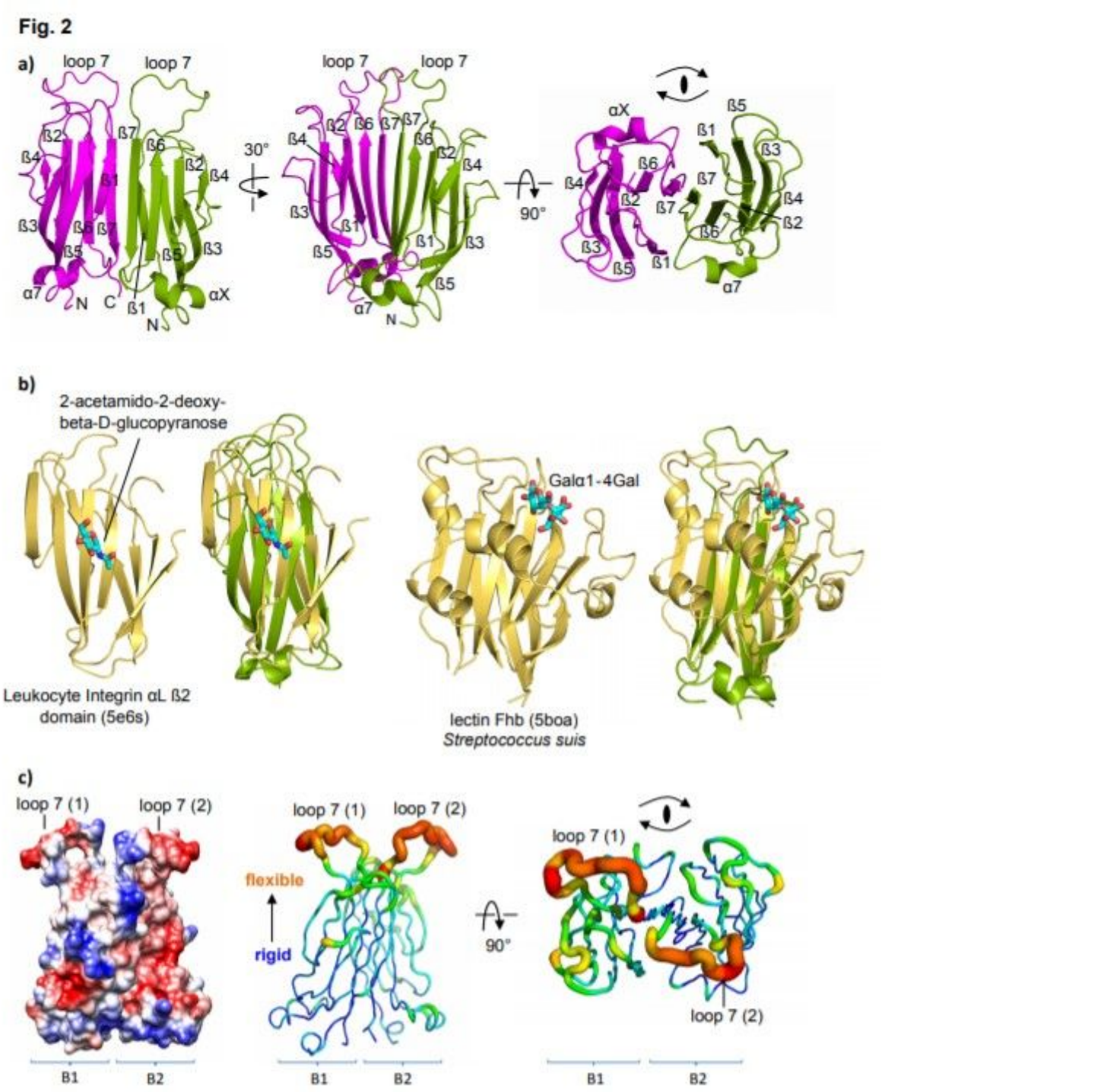


## Figure 2

EsaAex has structural similarity to bacterial lectins and eukaryotic integrins. The similarity of EsaAex to adhesive proteinS suggest a function in targeting bacterial prey or eukaryotic cells. A) Cartoon representation of the ß-sheet domain of EsaAex. Monomer 1 is shown in green and monomer 2 in pink B) Left: Superimposition of the ß-sheet domain (Mon1, green) with Leukocyte Integrin αL ß2 domain (yellow; pdb ID 5e6s) bound to 2-acetamido-2-deoxy-beta-D-glucopyranose (cyan). Right: Superimposition of the

ß-sheet domain (Mon1, green) with lectin Fhb (yellow; pdb ID 5boa-E) Streptococcus suis bound to alpha-D-galactopyranose-(1-4)-beta-D-galactopyranose (cyan). C) Coulomb surface potential representation of the EsaAex ß-sheet domain. D) Sausage representation of the temperature factor (B-factor) of the EsaAex ß-sheet domain. Increasing flexibility is indicated by the color gradient (blue, lowest to red, highest) and the increasing model diameter.

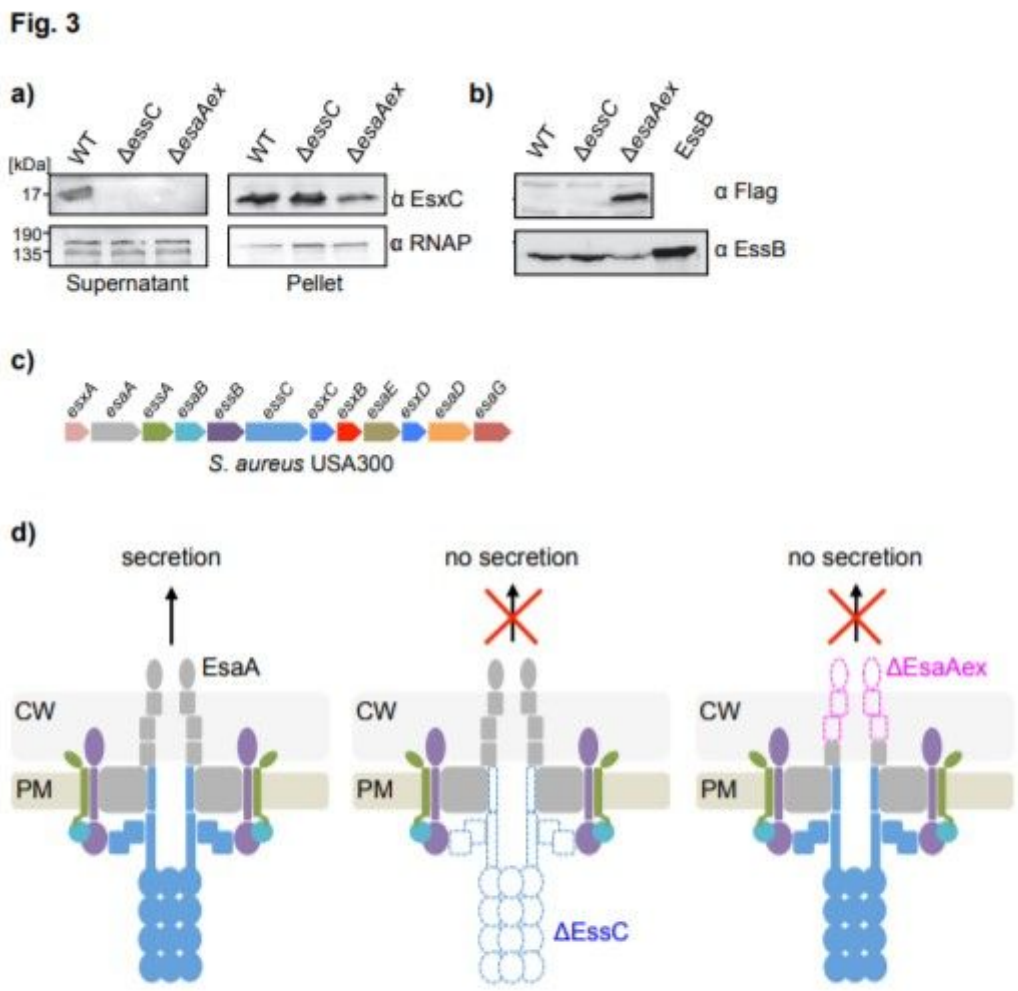


## Figure 3

The extracellular domain of the EsaA has a critical function in secretion. A) S. aureus USA300 wild type (WT) secretes effector proteins EsxC into the culture medium. In contrast, S. aureus USA300 lacking either the extracellular domain of EsaA (ΔesaAex) or the EssC motor ATPase (ΔessC) fail to secrete EsxC. Supernatant (left) and membrane pellet (right) of S. aureus USA300 wild type, ΔessC and ΔesaAex were analyzed by Western Blot. Loading controls (left panel) & lysis controls (right panel): RNA polymerase ß (RNAP, ca. 150 kDa). B) Western Blot analysis of the membrane fraction of S. aureus USA300 WT, ΔessC

and ΔesaAex shows expression of EssB and EsaAΔesaAex (containing 3x flag tag). C) Schematic of the T7SSb gene cluster from S. aureus USA300. D) Schematic of the T7SSb representing the results the secretion assay.

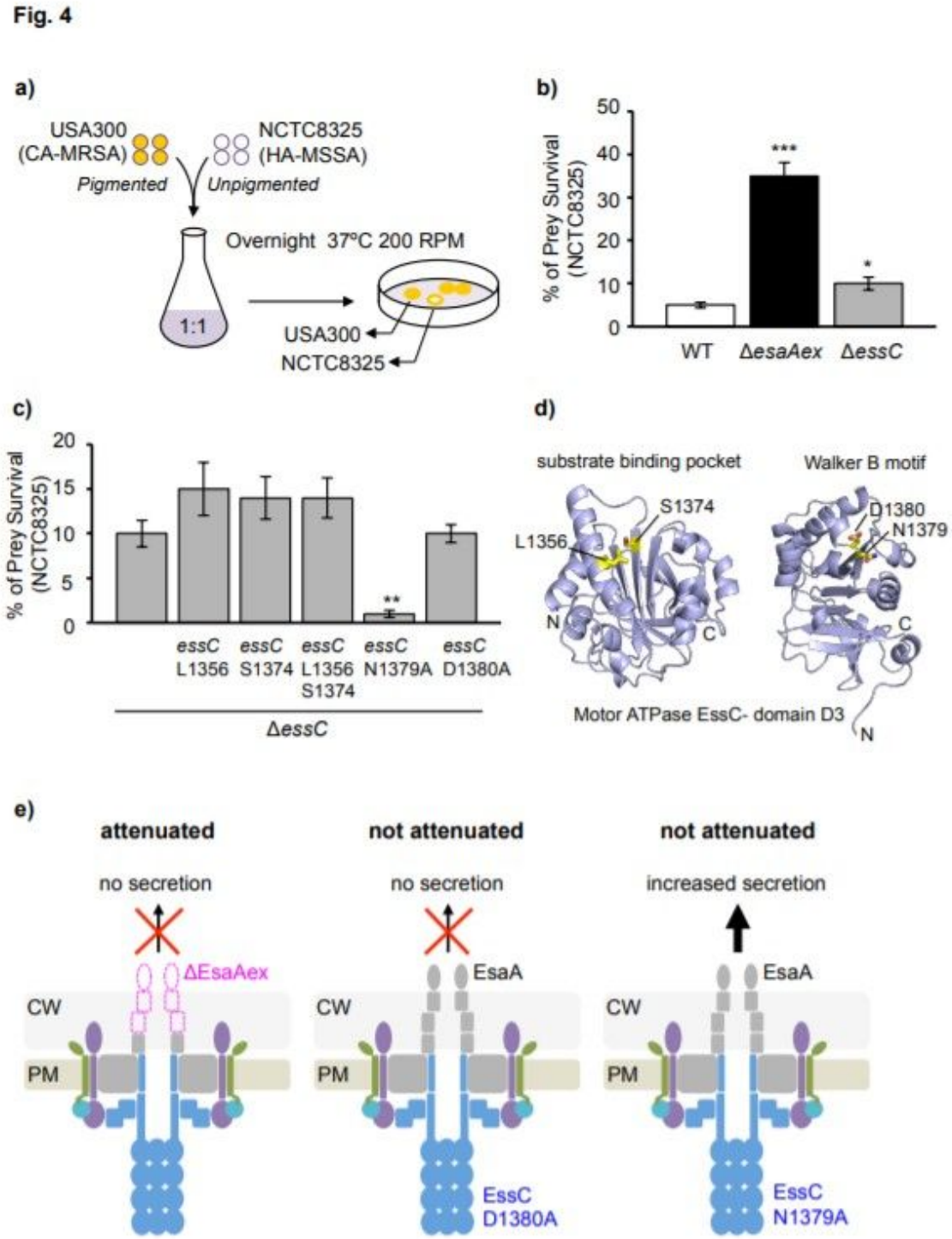


## Figure 4

The extracellular domain of the EsaA is required for antibacterial activity. In vitro growth competition assays between S. aureus USA300 and the prey strain S. aureus NCTC8325 in liquid medium show that

S. aureus USA300 ΔesaAex kills prey bacteria less efficient in comparison to S. aureus USA300 ΔessC. A) Schematic of the competition assay B) % of prey survival (NCTC8325) in the bacterial competition assay. Strains USA300 and NCTC8325 were mixed at 1:1 concentration and incubated overnight before plating and colony count. In the control mix (left column, NCTC8325 wt + USA300 wt), less than the 10% of the total population of NCTC8325 survived overnight incubation with USA300. However, when NCTC8325 wt was mixed with USA300 ΔesaAex mutant, approximately 40% of the total population survived USA300 co-incubation whereas the % survival of NCTC8325 population was more than 10% when incubated with USA300 ΔessC mutant. Comparisons were made using the unpaired Student t test; ***$p<0.001$ and *$p<0.05$. C) % of prey survival (NCTC8325) in the bacterial competition assay when co-incubated with different USA300 strains. USA300 ΔessC or ΔessC strains complemented with variants of EssC were mixed with NCTC8325 were mixed at 1:1 concentration and incubated overnight before plating and colony count. Comparisons were made using the unpaired Student t test; **$p<0.01$. D) crystal structure of the substrate recognition domain D3 of the EssC motor ATPase showing crucial amino acids in the substrate (left) and nucleotide binding sites (right). E) Schematic of the T7SSb representing the results the competition assay.

Fig. 5

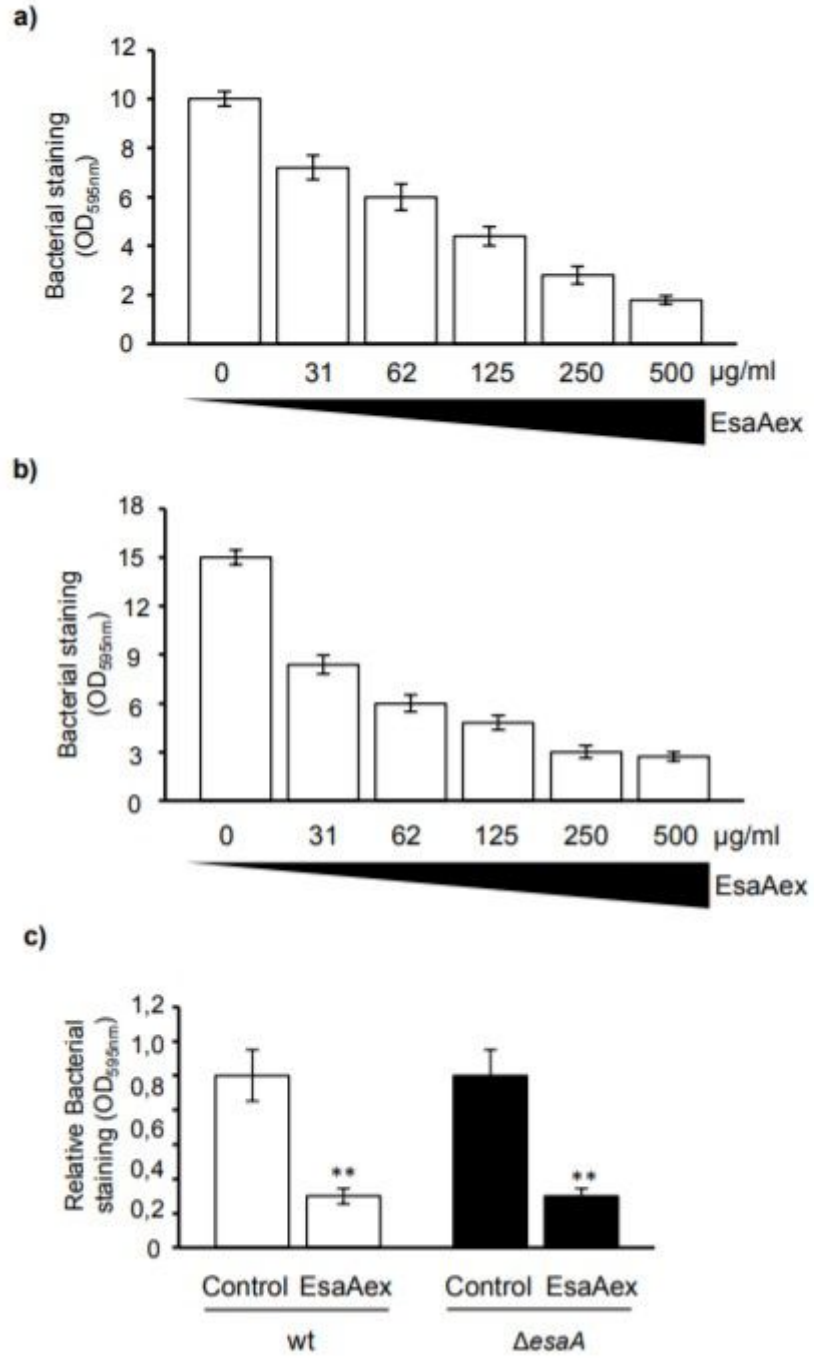


## Figure 5

The extracellular domain of EsaA interferes with biofilm formation. Addition of increasing concentrations of EsaAex affect growth in S. aureus static cultures cultures of NCTC8325 and USA300. Cultures were grown in TSB supplemented with NaCl 0,5% and Glucose 3% and incubated overnight at 37°C and incubated with different concentrations of EsaEx (0, 31, 62, 125, 250 and 500 µg/ml). In cultures supplemented with 0 µg/ml, the EsaAex solution buffer was added. A) Static cultures of NCTC8325 at different concentrations of EsaEx. B) Static cultures of S. aureus USA300 at different concentrations of

EsaEx. C) Static cultures of S. aureus USA300 wt and ΔesaA mutant supplemented with 250 µg/ml of purified EsaEx. The killing effect associated with EsaA was detected in different strains and is independent of EsaA expression.

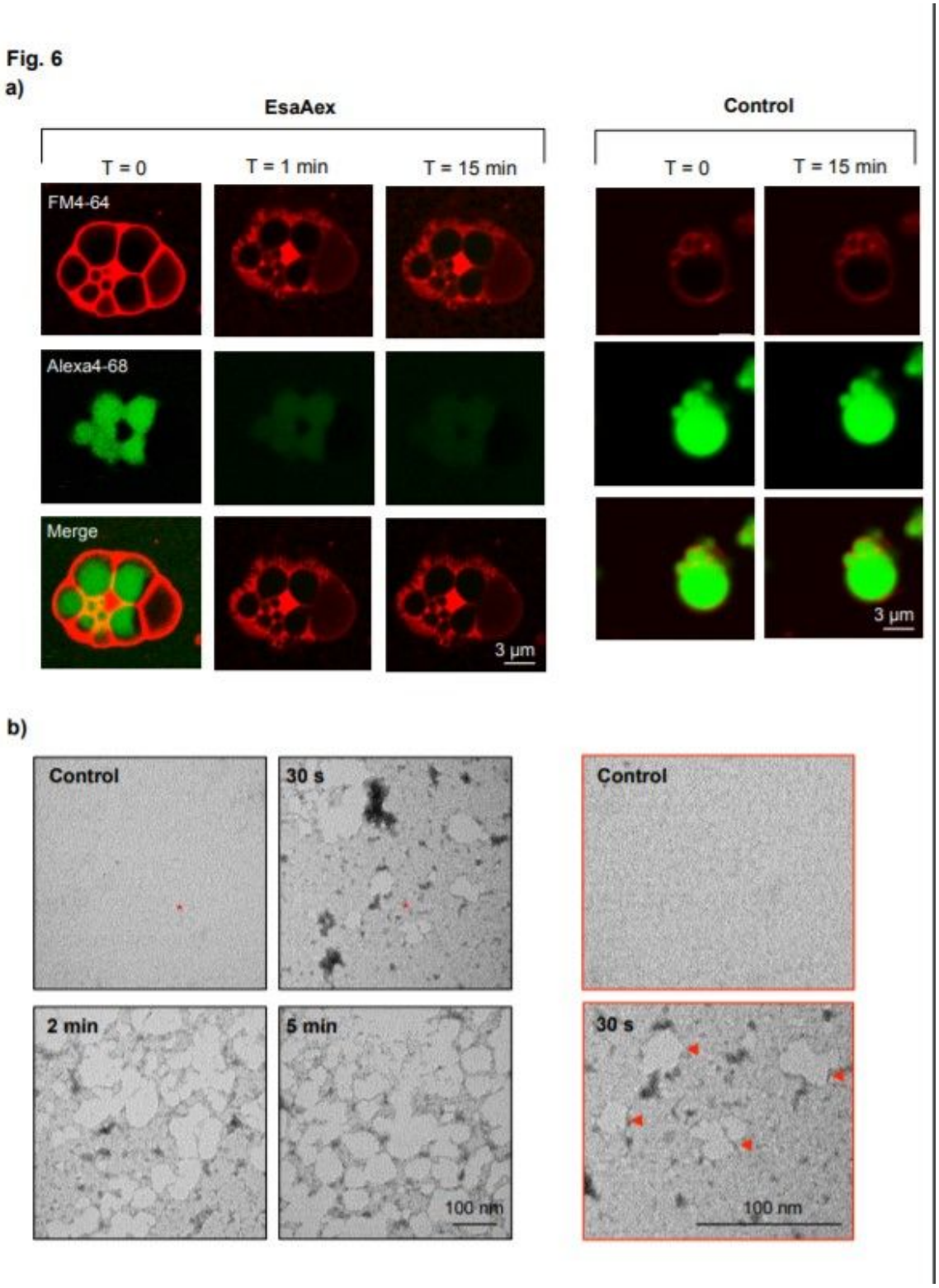


## Figure 6

EsaAex has phospholipid membrane damaging activity. A) Addition of purified EsaAex causes the efflux of Alexa488 out of giant unilamellar vesicles (GUVs). GUVs membrane staining was performed using the

membrane dye FM4-64. The disintegrating of GUV's was monitored over time using confocal microscopy. Membrane damage of the GUVs causes the release of the stained solution and thus, GUVs loses the internal green fluorescence signal. When GUVs were incubated with control buffer, the internal green fluorescence signal remained constant over time. B) Addition of purified EsaAex to lipid monolayers leads to disintegration of lipid monolayers. The membrane disrupting activity of EsaA was monitored over time using negative stain EM.

## Supplementary Files

This is a list of supplementary files associated with this preprint. Click to download.

- SupplementaryInformation.docx
- SuppFiguresfinal.pdf